

# Convection and fluidization in oscillatory granular flows: The role of acoustic streaming

Jose Manuel Valverde<sup>a</sup>

Faculty of Physics, University of Seville, Avenida Reina Mercedes s/n, 41012 Seville, Spain

Received 28 January 2015 and Received in final form 13 April 2015

Published online: 30 June 2015 – © EDP Sciences / Società Italiana di Fisica / Springer-Verlag 2015

**Abstract.** Convection and fluidization phenomena in vibrated granular beds have attracted a strong interest from the physics community since the last decade of the past century. As early reported by Faraday, the convective flow of large inertia particles in vibrated beds exhibits enigmatic features such as frictional weakening and the unexpected influence of the interstitial gas. At sufficiently intense vibration intensities surface patterns appear bearing a stunning resemblance with the surface ripples (Faraday waves) observed for low-viscosity liquids, which suggests that the granular bed transits into a liquid-like fluidization regime despite the large inertia of the particles. In his 1831 seminal paper, Faraday described also the development of circulation air currents in the vicinity of vibrating plates. This phenomenon (acoustic streaming) is well known in acoustics and hydrodynamics and occurs whenever energy is dissipated by viscous losses at any oscillating boundary. The main argument of the present paper is that acoustic streaming might develop on the surface of the large inertia particles in the vibrated granular bed. As a consequence, the drag force on the particles subjected to an oscillatory viscous flow is notably enhanced. Thus, acoustic streaming could play an important role in enhancing convection and fluidization of vibrated granular beds, which has been overlooked in previous studies. The same mechanism might be relevant to geological events such as fluidization of landslides and soil liquefaction by earthquakes and sound waves.

## 1 Acoustic streaming

Acoustic streaming was firstly reported in 1831 Faraday's seminal paper [1]. The patterns acquired by low-inertia fine particles (lycopodium powder) sprinkled on vibrating plates helped Faraday to trace the trajectories of steady circulation currents developed in the surrounding fluid. Almost half a century after Faraday's paper, Taylor (1878) [2] observed whirling air currents above horizontal films adhered to the aperture of a resonator tube which was subjected to sonorous vibrations. A similar phenomenon was contemporarily inferred by Dvorak (1874) [3] from the accumulation of dust particles inside a tube set into vibration at one end and closed at the other (Kundt's tube). Later on, steady streaming cells inside Kundt's tube were photographed by Andrade (1931) [4] using tobacco smoke particles as flow tracers. Figure 1 shows the acoustically induced steady streaming inside a Kundt's tube, which can be clearly visualized nowadays by means of Particle Image Velocimetry. Andrade [4] also discovered that any particle with sufficiently large inertia not to be entrained by the vibratory motion of a viscous fluid may be the center of a fluid vortex motion. Figure 2a is a photograph shown by Andrade, which illustrates the time-independent streaming flows developed

around a small solid sphere subjected to the sound wave generated by a loudspeaker. Similar streaming cells can be seen around liquid droplets levitated by an ultrasonic wave [5] (fig. 2b).

The fundamental physics that drives acoustic streaming was firstly envisaged by Lord Rayleigh (1884) [6] who found a second-order solution to the Navier-Stokes equations for the motion of a viscous fluid adjacent to an oscillating solid plane. The time-averaged solution of the Lagrangian velocity field reveals a secondary motion of the fluid in the form of steady (time-independent) vortices located between nodes and antinodes [7] and resulting from the frictional dissipation of energy in a boundary layer nearby the solid. Vorticity diffuses away from the solid over a depth

$$\delta \sim \sqrt{\frac{\nu}{\omega}}, \quad (1)$$

where  $\nu$  is the kinematic viscosity,  $\omega = 2\pi f$ , and  $f$  is the oscillation frequency. Further theoretical analysis by Schlichting [8] showed the development of near boundary steady vortices adjacent to the solid plane of size  $(\lambda/4) \times 2.7\delta$  (Schlichting or inner streaming).

The problem of a sound wave impinging on a circular cylinder or a sphere of radius much smaller than the wavelength ( $R \ll \lambda$ ) is also tractable analytically in the limit of small oscillation amplitude ( $\xi_1/R \ll 1$ ) [9–13].

<sup>a</sup> e-mail: jmillan@us.es

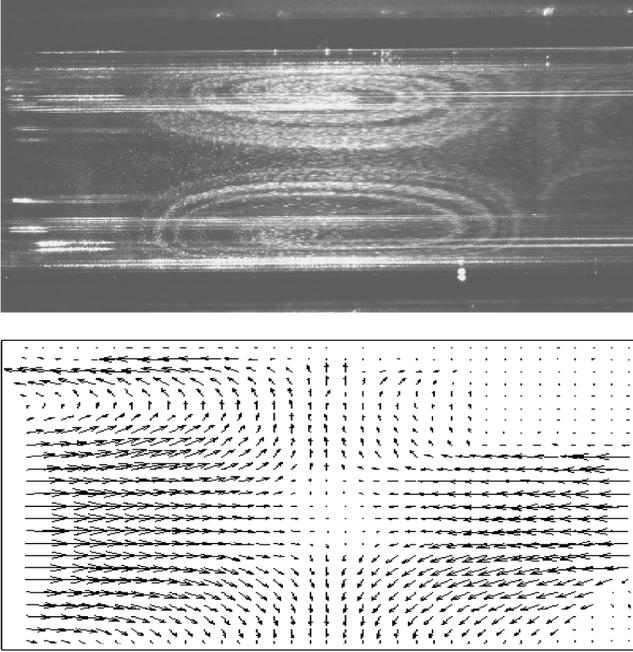


**Fig. 1.** Acoustic streaming inside a Kundt's tube recently observed by means of Particle Image Velocimetry (PIV). A sound wave inside the tube (1975 Hz) was generated by a horn loud-speaker driver corresponding to the seventh normal mode of the air column. The top figure shows the fluid flow trajectories as traced by fine particles and using a beam of laser optically expanded into a two-dimensional light sheet, which is focused by means of a CCD fast camera. The bottom figure is a velocity map derived from another PIV image. Reproduced from [104] with permission.

This ensures that the oscillatory fluid particles transverse very short distances relative to the solid, thus the flow remains attached to the body and laminar. An equivalent problem would be that of a solid undergoing small amplitude oscillations in a viscous fluid otherwise at rest. The characteristic velocity of the steady streaming flow around the object is

$$u_s = \frac{u_1^2}{\omega R} = \left( \frac{\xi_1}{R} \right) u_1, \quad (2)$$

where  $u_1 = \xi_1 \omega$  is the oscillation velocity amplitude. Thus, the fluid flow field around the body is determined by the streaming Reynolds number

$$Re_s \equiv \frac{u_s R}{\nu} = \left( \frac{\xi_1}{\delta} \right)^2. \quad (3)$$

The common situation in acoustics is  $R/\delta > 1$ . Then an inner boundary layer is formed of thickness  $\sim \delta$  wherein the motion of the fluid assumes a hemispherically symmetric recirculatory pattern (see figs. 2c-d). The streaming velocity remains on the order of  $u_s$  at the edge of this boundary layer where it plays the role of a slip velocity in driving an outer streaming flow. If  $Re_s < 1$ , the fluid recirculates outside the boundary layer (outer or Rayleigh streaming) with a characteristic vortex size only limited by the confinement [14, 15]. On the other hand, for  $Re_s > 1$ ,

the outer streaming assumes the form of a boundary layer of thickness  $\sim \delta(R/\xi_1)$ , which is larger than the inner boundary layer depth but still small as compared to the body size. The streaming velocity in the outer boundary layer remains on the order of  $u_s$  and decays to zero beyond it [12]. In the case of low-frequency oscillations (in the range of tens of hertz), the inner boundary layer thickness in air is of the order of hundreds of microns. For particles of small size ( $R/\delta < 1$ ) no boundary layer is developed. Vorticity diffuses in this limit over a wide region as compared with the size of the body and, since the Reynolds number (defined in terms of  $u_1$ )

$$Re_1 = \frac{u_1 R}{\nu} \sim \left( \frac{\xi_1}{R} \right) \left( \frac{R}{\delta} \right)^2 \quad (4)$$

is small, the non-linear term  $((\mathbf{u} \cdot \nabla) \mathbf{u})$  in the Navier-Stokes momentum conservation equation can be neglected, which gives rise to a Stokes flow.

The characteristic velocity of acoustic streaming  $u_s$  is, for small oscillation amplitudes, smaller than the oscillation velocity amplitude (eq. (2)). In the case of large oscillation amplitudes ( $\xi_1/R > 1$ ), the streaming velocity would become higher than  $u_1$ . The problem is then approachable analytically but only for small Reynolds number ( $Re_1 < 1 \rightarrow R/\delta < 1$  for  $\xi_1/R > 1$ ), *i.e.* in the absence of boundary layer, which leads to a Stokes flow. In the case that a boundary layer is developed ( $R/\delta > 1$ ) and the amplitude of oscillations are large ( $\xi_1/R > 1$ ), the Reynolds number  $Re_1$  is also large and the flow becomes strongly non-linear, which requires a numerical solution of the conservation equations.

Sonoprocessed gas-fluidized bed reactors [16, 17], thermoacoustic refrigerators/engines [18], pulsating combustion [19], reactor fuel rods [20], acoustic levitation [14, 21], microfluidics [22, 23] and solar thermal collectors [24] are just a few examples of the many physicochemical processes influenced (intentionally or accidentally) by acoustic streaming, which can lead to a notable enhancement of the transfer of heat [25] and momentum [26] between the fluid and solid phases. In the limits  $\xi_1/R \ll 1$  and  $R/\delta \gg 1$ , an approximate solution of the Navier-Stokes momentum and energy conservation equations [13] shows that the Nusselt number ( $Nu = HL/\kappa$ , where  $L$  is a characteristic length of the solid,  $\kappa$  is the thermal conductivity of the fluid, and  $H$  is the heat transfer coefficient) scales as  $Nu \sim Re_s^m Pr^n$  where  $m \simeq 0.5$ ,  $Pr$  is the Prandtl number ( $Pr = \nu/\chi$ , where  $\chi$  is the thermal diffusivity) and  $m \simeq n \simeq 0.5$ . Thus, for  $Re_s \gg 1$  the strong convection associated to acoustic streaming intensifies significantly the heat transfer. This scaling law has been verified by empirical measurements obtained in a wide variety of experimental conditions [25, 27, 28]. On the other hand, acoustic streaming causes also an enhancement of momentum transfer that may be an important source of inefficiency in thermoacoustic devices based on the exchange of heat between the working gas and a porous solid (stack) [26].

Empirical observations on oscillatory viscous flows through porous media show (without a clear explanation provided) that the root mean square (rms) pressure drop

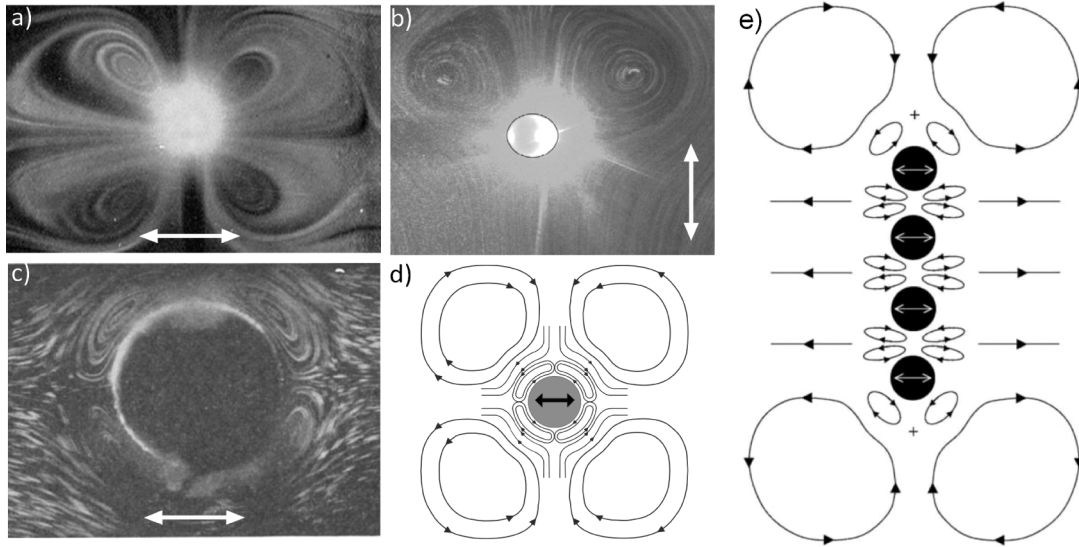


**Fig. 2.** a) Steady streaming of air around a 0.32 cm diameter sphere subjected to a sound wave generated by a loud speaker ( $f = 840$  Hz) and using tobacco smoke particles as flow tracers; reproduced from [4]. b) Steady air streaming around a water droplet ( $2 \mu\text{l}$  volume) levitated in air by an ultrasonic wave (58 kHz); reproduced from [5]. c) Inner steady streaming observed around a circular cylinder of radius 0.11 cm subjected to a standing sound wave ( $f = 200$  Hz); reproduced from [10]. d) Schematic representation of the theoretically predicted inner and outer steady streaming around a circular cylinder oscillating in the horizontal direction in a viscous fluid [11]. e) Schematic diagram showing the streaming flow for an oscillating chain of spheres as inferred from numerical simulations; reproduced from [37]. The double arrow indicates the direction of oscillation.

of a viscous oscillatory flow across a porous solid is several times higher than that due to a steady flow at similar Reynolds numbers [29–32]. The fundamental mechanism responsible for this behavior can be indeed found in acoustic streaming [33]. In the limit of small oscillation amplitude ( $\xi_1/R < 1$ ) or small Reynolds number ( $Re_1 < 1$ ) the drag force on an isolated sphere undergoing oscillations in a fluid with dynamic viscosity  $\mu$  is given by [11, 34]

$$F_1(t) = 6\pi\mu R \left(1 + \frac{R}{\delta}\right) u_1(t) + 3\pi R^2 \sqrt{2\mu\rho/\omega} \left(1 + \frac{2R}{9\delta}\right) \frac{du_1}{dt}, \quad (5)$$

which converges to the Stokes drag force ( $F_s = 6\pi\mu R u_1$ ) for  $R \ll \delta$ . For a system of non-interacting spheres subjected to an oscillatory flow, the rms pressure drop of the fluid per unit length would be

$$\frac{dp'_1}{dz} = n_0 \gamma F'_s, \quad (6)$$

$$\gamma = \left[ \left(1 + \frac{R}{\delta}\right)^2 + \left(\frac{R}{\delta}\right)^2 \left(1 + \frac{2R}{9\delta}\right)^2 \right]^{1/2}, \quad (7)$$

where  $n_0 = \frac{3\phi}{4\pi R^3}$  is the number of spheres per unit volume,  $F'_s = 6\pi\mu R u'_1$ ,  $u'_1$  is the rms oscillation velocity ( $u'_1 = u_1/\sqrt{2}$ ) and  $\phi$  is the volume fraction occupied by the spheres (packing density). The ratio of the rms pressure drop across the system to the pressure drop that would be due to a steady flow of superficial velocity  $u_g$

( $dp_g/dz = n_0 6\pi\mu R u_g$ ) is then

$$\frac{dp'_1}{dp_g} = \gamma \frac{u'_1}{u_g}. \quad (8)$$

In the limit  $R/\delta \gg 1$ , it is  $\gamma \simeq (2/9)(R/\delta)^2 \gg 1$ . Therefore, acoustic streaming in granular beds subjected to oscillatory viscous flows may lead eventually to a great enhancement of momentum transfer. In this limit, and for small oscillation displacements to keep the Reynolds number (eq. (4)) small, eq. (6) predicts values of the friction factor for oscillatory flows across porous media [35] in agreement with experimental measurements [30, 32, 36]. On the other hand, a numerical analysis would be required if the thickness of the viscous boundary layer is similar to the interparticle distance or smaller, which would lead to non-negligible hydrodynamic interactions. Recent simulations based on a numerical solution of the microscopic momentum and mass conservation equations within a simplified regular array of cylinders indicate that the interference between the boundary layers yields a further enhancement of viscous friction [33]. Figure 2d shows a schematic representation of the streaming flow around a vertical chain of spheres oscillating in the horizontal direction (inferred from numerical simulations [37]). As the spheres are brought together, the overlapping outer streaming cells with opposite circulations partially cancel. Numerical simulations and empirical observations demonstrate that when a vessel containing a water suspension of heavy beads initially clustered in the center is vibrated horizontally, the steady interstitial streaming flow leads

to the formation of chains oriented perpendicularly to the direction of vibration [37, 38].

## 2 Flow regimes in granular flows

This paper was started by describing the early evidences reported by Faraday on the vortex flow of air near vibrating plates as traced by fine powder particles that, because of their small inertia, became entrained in this steady circulation flow. Faraday observed a further peculiar phenomenon when looking at the effect of vertical vibrations on the dynamics of thick layers of large inertia sand grains. For sufficiently intense vibrations, the onset of convective currents of grains within the bulk of the bed was seen, eventually leading to the formation of surface heaps. Unlike lycopodium powder particles, individual sand grains could not be entrained by the gas flow when individually sprinkled on a vibrating plate due to their large inertia. Yet, Faraday observed that the interstitial fluid played an essential role on convection and surface heaping when deep beds of sand grains were vibrated [1]. A strong indication of the relevant role of gas effects was that convection disappeared when air was pumped out and appeared again as the air was readmitted. The study of vibration-induced convection in granular beds was resumed in the 1980s by Laroche *et al.* [39] who analyzed the behavior of vibrated beds of glass beads (of size in the range 0.6–0.8 mm), which indicated, as earlier inferred by Faraday, an important role of the interstitial gas on the onset of bulk convective motion and surface heaping. In agreement with Faraday's observations, Laroche *et al.* [39] observed that convection disappeared and the layer free surface remained flat when the experiment was carried out under vacuum ( $10^{-5}$  torr). The subject was amply debated in the late 1980s and early 1990s since the effect of interstitial air was questionable on the basis that the Stokes drag force is indeed not capable to sustain the weight of large inertia grains. Accordingly, gas effects were thought to be significant only for fine powders (particle size on the order of tens of microns) and other potentially relevant mechanisms were proposed as relevant for large inertia grains such as wall friction, boundary effects, phase variation or inhomogeneous forcing [40–43]. However, Pak *et al.* [44] carried out further observations using sand and glass beads that demonstrated again that granular convection and heaping in deep beds of large inertia grains disappeared when the gas was evacuated or when using permeable sidewalls. The later strongly suggested that the forced oscillations of a gas flow across the granular thick layer was a relevant mechanism as earlier inferred by Laroche *et al.* [39].

Chemical engineering studies have long reported that the effective fluid-solid drag coefficient is substantially increased in oscillatory flows as compared to that expected under steady conditions. Thus, the settling of large inertia beads is substantially slowed down in a vertically oscillating fluid. The measured retardation was much larger than that expected from the fluid-solid drag under steady conditions and in some cases the particles could be levitated

in the oscillating fluid [45–47]. Likewise, experimental results obtained in the context of thermoacoustic refrigerators and using diverse types of media (such as woven wire screens [29, 48], metal mesh screens and felts [30] and open-cell foams [32]) show that the root mean square pressure drop across a porous solid, as due to an oscillatory viscous flow, is several times higher than that due to a steady flow at the same Reynolds numbers [35]. Similarly, the viscous friction of oscillatory flows through pipes is notably greater than that expected for steady flows [31]. Thus, the fluid-particle interaction could be substantially enhanced in vibrated granular beds by the development of oscillatory flows as compared to steady flows, which would lead to an important role of the interstitial gas on the onset of convection and fluidization even in the case of large inertia grains. Nevertheless, it must be remarked that the role of interstitial gas on convective motion under oscillatory flows in vibrated granular beds does not rule out the possible effects of other mechanisms that might prevail under certain conditions as seen in some experimental works and simulations under reduced air pressure [39, 40, 43]. In particular, the behavior of vibrated sand piles might be very sensitive to the effect of boundaries [40]. For example, Laroche *et al.* [39] observed that heap formation could still be observed under vacuum but only at high frequencies and in narrow cells due to lateral boundary effects. Numerical simulations reported in the 1990s and based on molecular dynamics (MD) algorithms seemed to show that convection and fluidization in a vibrated bed would be generated by the viscoelastic interactions between the particles and friction with the walls in the absence of interstitial gas [49–51]. However, caution must be taken on identifying computer-generated patterns with experimental findings as pointed out in [52]. The appearance of convection rolls was shown in that work to be caused by limitations of the numerical method arising from the use of large contact times at collisions [52]. Convection patterns disappeared when the contact time between colliding particles was close to its physical value [52]. More recent numerical simulations based on the combination of granular dynamics (GD) and computational fluid dynamics (CFD) [53, 54] indicate that granular convection and heaping relies on the drag force due to the air flowing into (and out of) the void between the bed and container bottom.

Faraday also looked at the behavior of liquids on vibrated plates and discovered the formation of ripples (Faraday waves), which have been the subject of an extensive number of studies. More recently, it has been seen that, as the vibration intensity is increased beyond the onset of convection, vibrated granular beds exhibit also surface patterns strikingly resembling the Faraday waves in liquids (see fig. 5) [55]. The underlying mechanism driving the onset of convection and the liquid-like behavior of vibrated granular beds of large inertia grains is not clearly understood. One would be tempted to consider the granular bed as an effective fluid whose motion is determined by a set of differential equations (the equivalent to Navier-Stokes conservation equations for Newtonian liquids) and the corresponding boundary conditions.

Savage [56] made in 1988 an effort in this direction and considered the granular material in the continuum context as a compressible fluid characterized by an effective viscosity and a granular temperature related to the particle velocity fluctuations, which decayed away from the vibrated bed bottom due to inelastic grain-grain collisions. Accordingly, it was proposed that the circulatory motions observed in vibrated granular beds could be viewed as simply another example of acoustic streaming yet resulting from energy dissipation in the interior of the granular material. However, some of the experimental observations carried out extensively in the 1990s contradicted this continuum approach [41,57]. Moreover, although measurements of an effective granular viscosity and temperature of granular solids have been pursued in many works, the values obtained are anisotropic, inhomogeneous and unexplainably dependent on the history of the material and particular conditions of the experiment [58–60]. For example, the viscosity derived from both the free and forced oscillations of a rigid pendulum immersed in vibrated granular beds is strongly influenced by the probe shape and vibration frequency [60]. Thus, there is not a widely accepted granular-dynamics continuum theory but a variety of phenomenological models evidencing in some particular aspects stunning analogies with conventional fluids [61]. The key issue is that any continuum theory must be founded on an averaging of quantities over length and time scales macroscopically very small but much larger than microscopic relevant scales (in Newtonian fluids the typical size of the constituents molecules). Granular materials are however inherently heterogeneous over macroscopic scales larger than the size of the grains. Moreover, the correct boundary conditions for granular flows are unclear. Magnetic resonance imaging of vibrated granular beds has shown that the flow is fastest at a thin boundary layer near the wall [62], which contrasts with the no-slip boundary condition that applies for conventional viscous fluids.

Granular materials exhibit radically different behaviors depending on the physical properties of the particles and mainly their size. If particles are small (typically below  $100\ \mu\text{m}$ ), there is a strong hydrodynamic interaction between the interstitial gas and the particles of a granular bed that leads to fluidization at low Reynolds numbers [58, 63, 64]. Since the drag force of the air trapped within the bed on low-inertia fine particles easily counterbalances their weight, fine powders transit directly from the solid-plastic regime to the fluidization regime in any dynamical process if cohesiveness is not too strong, taking the appearance of a low-viscosity liquid such as water. Stresses in this liquid-like fluidization regime are mostly transmitted by the hydrodynamic gas-solid interactions. On the other hand, the dynamics of dry coarse granular materials such as sand (of grain size typically above  $100\ \mu\text{m}$ ) in air is usually governed by inertial forces which prevail over the drag force exerted by the interstitial air. When the frictional forces between the grains are overcome the bed enters an inertial convective regime commonly characterized by the onset of superficial avalanches. Stresses in this regime are mainly transmitted by iner-

tia and interparticle collisions whereas the gas-particle interaction is negligible. If, for example, air is pumped out from a rotating drum partially filled with sand the dynamics is not changed and the angle of avalanche is kept slightly over the angle of repose characteristic of the granular material [63]. Fluidization of coarse granular materials can be only achieved if air is forced to pass through the bed at very large Reynolds numbers [63]. Now, this general picture enters into conflict with empirical observations of bulk convection and liquid-like behavior in vibrated granular beds as influenced by gas effects. Despite the numerous efforts aimed at analyzing the physics that governs the avalanching behavior of vibrated granular beds in the inertial regime, the fundamental mechanism driving this behavior is not well understood yet [65]. A fundamental question is why gas effects could play still a relevant role on the behavior of large inertia particles at not large Reynolds numbers for which the Stokes drag force is small as compared to particle's weight. The next section is focused on analyzing acoustic streaming as a possible mechanism responsible for the enhancement of the gas-particle hydrodynamic interaction in vibrated thick layers of large inertia grains.

## 3 Role of acoustic streaming on oscillatory granular flows

### 3.1 Onset of convection and fluidization

When deep beds of granular materials are vibrated, the onset of convection is observed for a threshold value of the dimensionless vibration acceleration  $\Gamma = \Gamma_c = \xi_{1c}\omega^2/g \simeq 1$ , where  $g = 9.81\ \text{m}^2/\text{s}$  is the gravitational acceleration. At this critical acceleration, the bed is lifted when the effective gravity becomes negative, leaving a small gap between its bottom and the plate that is closed in the ascending part of the cycle, which gives rise to an oscillatory passage of gas through the bed flowing into and out of the gap and playing a determining role on the transition to the inertial convective regime as seen in many works [1, 39, 43, 44, 53, 54, 65, 66, 66–71]. Bulk convective currents give rise to the formation of a surface heap along which particles avalanche down to be subducted into the bed at its lowest point (see fig. 3). A remarkable result is that the slope of the surface heap sustains an angle with the horizontal smaller than the characteristic angle of repose of the material in the absence of vibration [72]. Furthermore, the angle of the slope decreases and additional convective rolls form as  $\Gamma$  is increased over  $\Gamma_c$ . If the pressure of the ambient gas is reduced progressively, the slope angle grows first to a maximum until a critical pressure below which convection disappears [65].

Besides the dimensionless vibration acceleration, a further parameter that intervenes in the process is the dimensionless vibration energy  $E = u_1^2/(gR) = \Gamma\xi_1/R$  [67, 73]. Empirical observations at low frequencies ( $f < 30\ \text{Hz}$ ) and in the range of particle size  $d_p \simeq 0.2\text{--}1\ \text{mm}$  show that it must be  $E \gtrsim \Gamma_c$  to sustain the convective circulation of

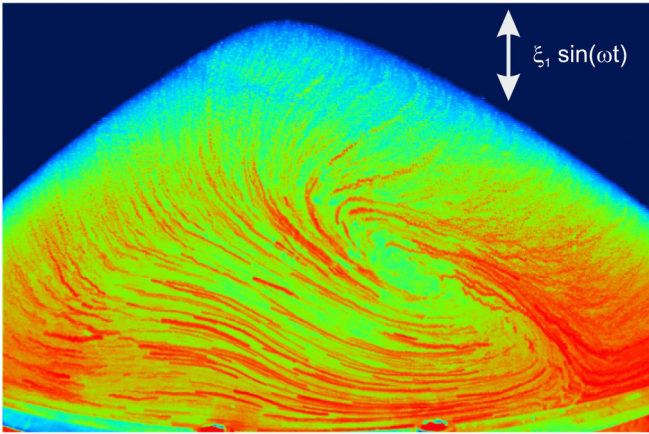


**Fig. 3.** Bulk convective flow and surface heaping experimentally observed in a vertically vibrated bed of sand ( $f = 10$  Hz,  $\xi_1 = 1$  cm). Photograph obtained by Robert Hartley and co-workers at Duke University (Robert Behringer's group) [65].

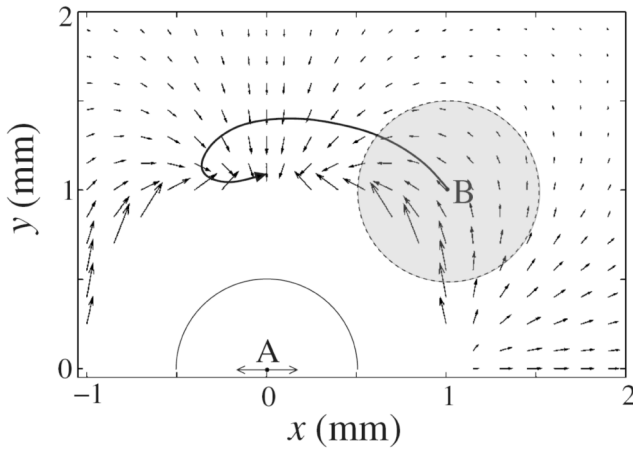


**Fig. 4.** Vectorial plot showing the magnitude and direction of the hydrodynamic force that acts at the center of a sphere  $B$  as a function of its position nearby another sphere  $A$ . Both spheres are oscillating in the horizontal direction (reproduced from [37]). The solid line indicates the trajectory of a particle  $B$  initially placed at  $(1, 1)$  if it were free to move. Calculated from numerical simulations as detailed in ref. [37].

particles [67]. Although other mechanisms such as wall friction or inhomogeneous forcing could still produce convection and surface heaping, the anomalously low dynamic avalanche angle and the influence of the gas pressure observed in many experiments [1, 39, 44, 72] suggests that in these situations the interstitial gas weakens interparticle friction. In an oscillating granular bed, we would expect that a steady streaming is developed in the interstitial space between the solid particles of characteristic velocity  $u_s \sim u_1^2/(\omega R) = u_1 \xi_1/R$  [33, 37]. The ratio of the steady streaming velocity to the oscillation velocity amplitude is  $u_s/u_1 \sim E/\Gamma$ . At the observed onset of convection ( $E \sim \Gamma_c \sim 1$ ) the intensity of the steady (non-zero time-averaged) streaming flow becomes comparable to that of the oscillating flow ( $u_s \sim u_1$ ). Figure 4 shows a vector plot obtained from numerical simulations [37] of the

steady hydrodynamic force acting on a sphere  $B$  nearby another sphere  $A$  caused by the steady streaming flow developed when both particles oscillate with the same amplitude in the horizontal direction. As may be seen, the interparticle hydrodynamic force depends on the alignment of the dimer relative to the direction of oscillation. The force is attractive when the pair is vertically aligned and repulsive in the oscillation direction whereas it is maximum and tangential when the spheres are aligned at an angle of  $\sim 45^\circ$  with the direction of oscillation [37]. Experiments and simulations [37, 38] show that particles are drifted by these hydrodynamic forces when the amplitude of oscillations is similar to or greater than particle radius. Expectedly, these shear hydrodynamic forces will be also present in a vertically vibrated granular bed and would act by weakening the frictional resistance at interparticle contacts eventually triggering a convective motion when  $\xi_1 \sim R$  ( $u_s \sim u_1$ ). As the amplitude of the oscillation is further increased (at fixed frequency), the ratio  $E/\Gamma$  is increased [67]. Therefore, the ratio  $\xi_1/R = u_s/u_1$  increases further, which would promote the intensity of convection. Thus, frictional weakening by hydrodynamic shear forces might explain the onset of convection and the decrease of the angle of the surface heap slope with the vibration intensity observed experimentally [72].

As  $\Gamma$  builds up over  $\Gamma_c$  the surface heap is seen to disappear at a critical  $\Gamma = \Gamma_w$  leaving its place to liquid-like surface patterns [61, 65, 66, 68, 71]. Surface patterns of vibrated granular beds and those of vibrated liquids firstly illustrated in Faraday's paper show a striking similarity (see fig. 5). The critical acceleration at the transition from the inertial regime to the liquid-like behavior is typically around  $\Gamma_w \simeq 2$  at  $f \sim 10$  Hz and increases with frequency for deep granular beds. In principle, one might attribute the onset of liquid-like behavior to fluidization of the bed as due to the oscillatory passage of gas across it. In agreement with this argument, similar liquid-like surface patterns are also observed when a pulsating gas flow (of superficial gas velocity  $u_g + u_1 \sin(\omega t)$ ) is passed through a granular bed in a container at rest (see fig. 5) [43, 55]. Surface patterns in this pulsated bed are directly linked to fluidization since they appear at pulsation velocities greater than the minimum fluidization velocity  $u_{mf}$  [55]. Moreover, the characteristic size of surface waves in vibrated and pulsated fluidized beds varies linearly with  $1/f^\gamma$  ( $\gamma \sim 1-2$ ) [55, 68, 74, 75] in accordance with the dispersion relation of surface waves of low-viscosity liquids [34].

The possibility that the oscillatory flow through a vibrated granular bed could play a role on either the convective or fluidization regimes at the common conditions of vibrated bed experiments has been dismissed in previous works on the basis of the large inertia of the particles usually employed [44]. Using the same set of typical parameters in the convective regime as Pak *et al.* [44] in their study to support this argument ( $\rho_p = 3000$  kg/m<sup>3</sup>,  $d_p = 2R = 0.65$  mm for the density and size of the particles, respectively,  $\mu = 1.77 \times 10^{-5}$  Pa s,  $\rho = 1.18$  kg/m<sup>3</sup>,  $\xi_1 = 3$  mm,  $f = 10$  Hz,  $u_1 = \xi_1 2\pi f \simeq 0.2$  m/s,  $\Gamma \simeq 1.4$ ), the ratio of the Stokes force  $F_s = 6\pi\mu R u_1$  to particle

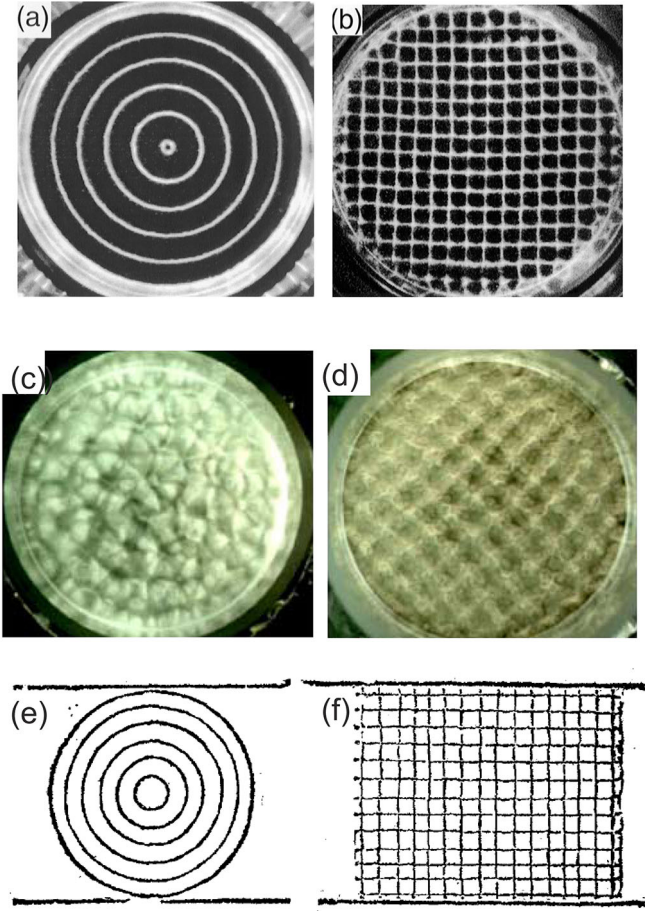


**Fig. 5.** a) and b): Surface patterns displayed by vibrated layers of 150–180  $\mu\text{m}$  diameter bronze spheres [89] (a:  $f = 28$  Hz,  $\Gamma = 3$ ; b:  $f = 17$  Hz,  $\Gamma = 2.5$ ). c) and d): Surface patterns in granular beds fluidized by a pulsatile flow of air with superficial velocity  $u(t) = u_g + u_1 \cos(\omega t)$  ( $u_1 = 0.9u_g$ ,  $f = \omega/2\pi \simeq 10$ –20 Hz, and  $u_g \simeq 3u_{mf}$ , where  $u_{mf}$  is the minimum fluidization velocity); reproduced from [55]. e) and f): Original drawings illustrated in Faraday's paper (1831) showing surface patterns of liquids upon vibrating plates [1].

weight is  $F_s/W_p \sim 0.05$ , which is indeed very small. However, neither hydrodynamic interactions within the granular bed nor acoustic streaming due to the oscillatory viscous flow are considered in this simple estimation.

Fluidization of a granular bed is due to the increase of the fluid pore pressure over atmospheric pressure. The fluid pressure drop  $\Delta p$  reduces the effective normal stress  $\sigma_{ef} = \sigma - \Delta p$ , where  $\sigma$  is the powder weight per unit area  $\sigma = \rho_p \phi g L$  and  $L$  is the thickness of the granular bed (fluid density is neglected). Thus, the bed loses mechanical strength and transits to a fluidized state when the fluid pressure drop per unit length balances the material weight per unit volume. The fluid pressure drop per unit length across a granular bed subjected to a steady fluid flow can be obtained from the Carman-Kozeny equation [76, 77]

$$\frac{dp_g}{dz} = E \frac{\phi^2}{(1-\phi)^3} \frac{\mu}{d_p^2} u_g, \quad (9)$$

where  $E$  (Ergun constant) is an empirical constant depending on particle's sphericity  $\Psi$  ( $E \simeq 180/\Psi$ ) and  $u_g$  is the superficial gas velocity. Equation (9) was originally derived by modeling a granular bed as a group of capillaries of diameter  $d_p$  parallel to the direction of flow. Its validity is restricted to the limit of low Reynolds number based on the gas velocity ( $Re_g = u_g R/\nu < 1$ ). Note that this equation can be rewritten as

$$\frac{dp_g}{dz} = \Lambda n_0 F_s, \quad (10)$$

where  $F_s = 6\pi\mu R u_g$  and  $n_0 F_s$  would be the pressure drop per unit length across an assembly of hydrodynamically non-interacting particles. The factor  $\Lambda \simeq 10\phi/(\Psi(1-\phi)^3)$  serves to correct the pressure drop for the hydrodynamic interactions within the bed and the shape of the particles, which cause an increase of the viscous friction as compared to an ideal system of non-interacting spheres ( $dp_g/dz = n_0 F_s$ ).

In the case of an oscillatory flow through a granular bed, the streaming flow cells developed around neighbor particles will interact. As seen in recently reported numerical simulations [33] this interaction leads to an increase of the rms pressure drop over the expected value for the case of non-interacting spheres (eq. (6)). Let us assume that, in the limit of small Reynolds number, the rms pressure drop per unit length  $dp'_1/dz$  of an oscillatory flow across a granular bed is corrected by the same factor  $\Lambda$  used for a steady flow. Using eq. (6) it is then

$$\frac{dp'_1}{dz} = \Lambda \Gamma n_0 F'_s. \quad (11)$$

By equating the gas pressure drop per unit length (eq. (11)) to the bed weight per unit volume ( $\rho_p \phi g$ ), the rms minimum fluidization velocity is obtained as

$$u'_{1mf} = \frac{u_t}{\Lambda \Gamma}, \quad (12)$$

where  $u_t = \rho_p g d_p^2 / (18\mu)$  is the Stokes settling velocity. Here it is assumed that the convective flow of the particles preceding fluidization is slow in comparison to the oscillatory flow as seen experimentally [78]. Another simplifying assumption is that particle collisions do not play a role on the viscous friction by disturbing the interstitial streaming flow. Further numerical work should be devoted to take into account these issues as well as to analyze the dependence of the hydrodynamic correction factor  $\Lambda$  on the packing density and shape of the particles. Our main goal is to open a debate on the importance of acoustic streaming in oscillating granular beds for the onset of convection and fluidization and motivate the necessity that numerical studies on realistic systems take into account acoustic streaming.

According to eq. (12) hydrodynamic interactions and acoustic streaming in oscillatory flows reduce the minimum fluidization velocity by a factor  $1/(\Lambda \Gamma)$  on the terminal settling velocity of an individual particle. For a randomly packed bed of spherical beads ( $\Psi = 1$ ,  $\phi \simeq$

0.6 [79, 80]) and using the same set of values for standard physical parameters in the convective regime as above, it is  $\Upsilon \simeq 2$  and  $\Lambda \simeq 90$  whereas the rms minimum fluidization velocity is  $u'_{1mf} = 0.22$  m/s, which is slightly larger than the rms oscillation velocity ( $u'_1 = 0.14$  m/s) but smaller than the characteristic streaming velocity  $u_s \simeq 1.8$  m/s. Thus, the steady streaming at these conditions would be sufficiently intense as to drive the observed convection ( $u_s/u_1 = E/\Gamma \simeq 10$ ). If the amplitude of vibration is increased,  $u'_1$  reaches the minimum fluidization velocity at  $\xi_1 = 4.7$  mm for  $\Gamma \simeq 2.1$ , which is about the value typically observed for the onset surface waves at low frequency and particles of similar size [67].

### 3.2 Effect of particle's shape and packing density

If the irregular shape of the particles is taken into account, the minimum fluidization velocity would be further decreased by a factor equivalent to the particle's sphericity. For example, in the case of sharp sand grains it is  $\Psi \simeq 0.66$  [81] even though a decrease of sphericity leads also to a decrease of the packing density. Hoffmann and Finkers [82] reviewed a large number of data reported in the literature on beds of particles in a wide range of sizes (up to a few millimeters) and packing densities and arrived at the empirical relationship  $\phi \simeq \phi_s \Psi^c$ , where  $c \simeq 0.85$  and  $\phi_s$  is the packing density for spherical particles. For a random loose-packing of sharp sand grains, it would be  $\phi \simeq 0.42$ . The packing density can be also influenced by initial compaction at small vibration amplitudes [83] albeit in the convective inertial regime preceding fluidization it will be decreased by dilation (Reynolds' dilatancy) [84]. Recently reported X-ray tomography visualization of shear flows shows that the reduction of packing density is a function of particle's shape. In the case of a random packing of spheres,  $\phi$  is decreased to about 0.5 in the shear zone [85]. In a vibrated granular bed the overall decrease of the packing density would depend on the relative size of the avalanching layer as compared to the bed height  $h$ . Using experimental data on the dilation of vibrated granular layers in the convective regime ( $\Delta h/\xi_1 \sim \Gamma$  for  $\Gamma > 1$ , see fig. 5 of [86]) the relative decrease of the packing density can be adjusted by the law  $\Delta\phi/\phi \simeq \Gamma\xi_1/h = ER/h$  (the tests reported in [86] were carried out for  $\Gamma = 1-2.7$ ,  $d_p = 0.05-1.0$  mm,  $h/d_p = 80-140$ ,  $\xi_1 = 0.66-6.65$  mm,  $f = 30$  Hz). Thus, dilatancy would be expected to be most significant for thin layers. Other parameters affecting the packing density can be particle size polydispersion, the geometry of the container and deposition method. In the derivation of eq. (12) an ideally unbounded bed has been assumed, which will be approximately the case of beds of size much larger than particle size. Otherwise, the shape of the container and depth of the granular bed would have a significant influence on the onset of convection and transition to fluidization as seen experimentally in some cases [43, 75].

### 3.3 Minimum fluidization acceleration

According to eq. (12), the minimum fluidization dimensionless acceleration ( $\Gamma_{mf} = \sqrt{2}u'_{1mf}\omega/g$ ) could be generally written as

$$\Gamma_{mf} = \sqrt{2} \frac{\omega\tau}{\Lambda\Upsilon}, \quad (13)$$

where  $\tau = \rho_p d_p^2 / (18\mu)$  is the particle relaxation time. Relatively large particles (typically  $d_p > 100 \mu\text{m}$ ) act as obstacles to the oscillatory gas flow ( $\omega\tau \gg 1$ ) [87], which will give rise to acoustic streaming on their surface that expectedly would favour fluidization. Thus, a simplified picture may be envisioned in which the bed would enter a streaming weakened inertial regime at the onset of convection ( $\Gamma_c \simeq 1$ ) after which at  $\Gamma = \Gamma_{mf}$  the bed transits to the fluidized regime and acquires a liquid-like state.

The values of  $\Gamma_{mf}$  obtained from eq. (13) would serve to predict the critical acceleration at the onset of liquid-like behaviour. In the standard range of frequencies used in vibration experiments ( $f \sim 10-100$  Hz), eq. (13) predicts a roughly linear increase of  $\Gamma_{mf}$  with frequency in qualitative agreement with experimental observations on the critical acceleration  $\Gamma_w$  at which surface liquid-like patterns appear in deep granular beds [66, 68, 71, 75]. A quantitative comparison with experimental results reported in the literature is difficult, however, for several reasons such as the absence of information on the shape of the particles and packing density, and the influence of non-ideal factors such as boundary conditions, size polydispersion, strongly non-linear effects (in the case  $\xi_1/R > 1$  and  $Re_1 > 1$ ), acoustic streaming interactions, dilation as depending on vibration intensity and bed depth, etc. Nevertheless, predicted data from eq. (13) have been plotted in fig. 7 along with experimental data of  $\Gamma_w$  extracted from several experimental works reported in the literature [66, 68, 75]. Despite the already mentioned uncertainties and the simplicity of the model, it is seen that the predicted curves for  $\Gamma_{mf}$  adjust satisfactorily well to experimental data on  $\Gamma_w$  for reasonable values of the packing density and particle's sphericity according to the materials and experimental conditions reported. On the other hand, experimental observations on shallow beds (usually of depth  $h < 10d_p$ ) [68, 88, 89] show that  $\Gamma_w$  is relatively high at low frequencies and remains more or less constant and independent of frequency. In shallow beds, the pressure drop would be expectedly smaller than that predicted by eq. (9). Moreover, since at low frequencies the amplitude of oscillations  $\xi_1$  can be much larger than particle size [67], it will be also larger than the bed depth. Thus, gas molecules have enough time to cross the whole bed during half a cycle, which will hinder the development of oscillatory flows within the bed. In the absence of these oscillatory flows, acoustic streaming will be prevented, which might explain the observed suppression of convection and heaping phenomena for shallow beds [44, 68, 74, 86, 90, 91]. Surface waves in vibrated shallow beds of large inertia particles are also observed under low air pressure but would be driven in that case by other mechanisms such as collisions with the bottom wall [74, 92].

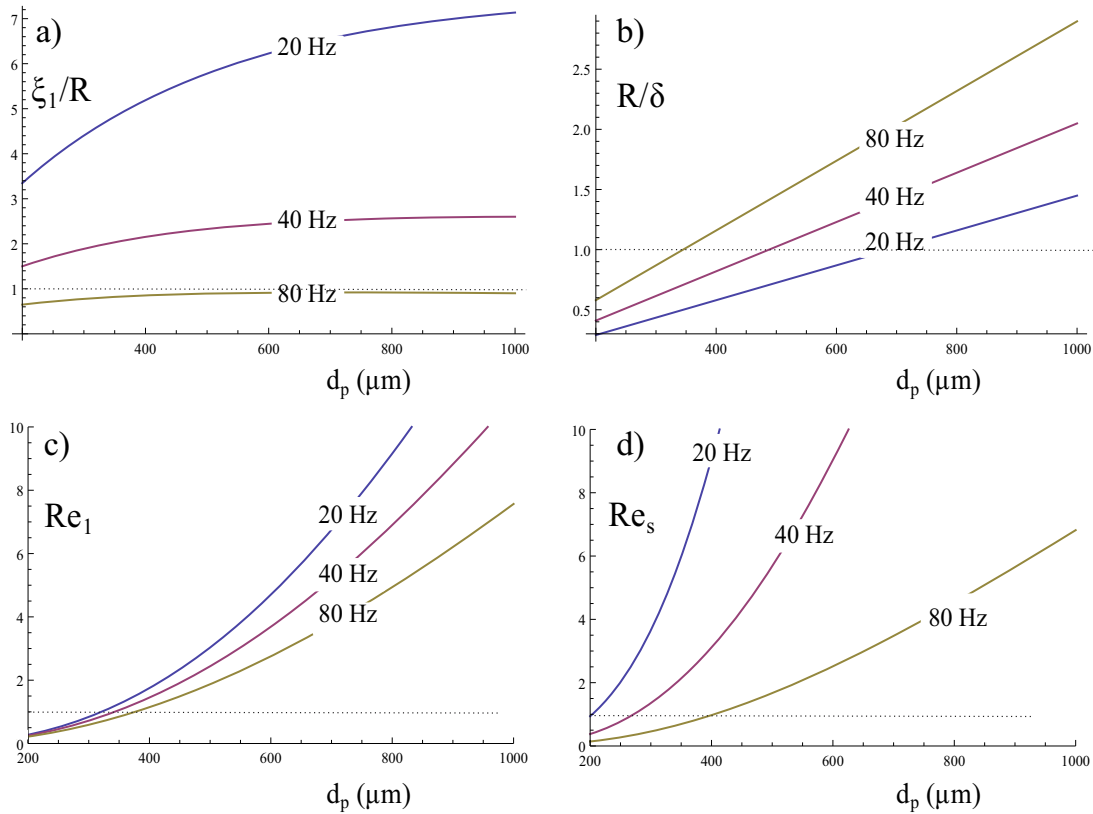


**Fig. 6.** a) Ratio of oscillation amplitude to particle radius ( $\xi_1/R$ ); b) Ratio of particle radius to Stokes layer thickness ( $R/\delta$ ); c) Reynolds number ( $Re_1$ ) and d) streaming Reynolds number ( $Re_s$ ) at minimum fluidization. Calculated values for  $\Psi = 1$ ,  $\phi = 0.6$ ,  $\rho_p = 3000 \text{ kg/m}^3$ ,  $\mu = 1.77 \times 10^{-5} \text{ Pa s}$ ,  $\rho = 1.18 \text{ kg/m}^3$ .

Figures 6(a,b,c,d) show the ratio of oscillation amplitude to particle radius ( $\xi_1/R$ ), ratio of particle radius to the Stokes layer thickness ( $R/\delta$ ), Reynolds number ( $Re_1$ ) and streaming Reynolds number ( $Re_s$ ) at predicted minimum fluidization conditions as a function of particle size ( $d_p = 0.2\text{--}1 \text{ mm}$ ) and for several vibration frequencies (using  $\Psi = 1$ ,  $\phi = 0.6$ ,  $\rho_p = 3000 \text{ kg/m}^3$ ,  $\mu = 1.77 \times 10^{-5} \text{ Pa s}$ ,  $\rho = 1.18 \text{ kg/m}^3$ ). For oscillation frequencies above a certain value, it is  $\xi_1/R \lesssim 1$  and  $R/\delta \gtrsim 1$ . At these conditions an inner boundary layer is expected to be developed around the surface of an individual particle. At low frequencies, it is  $\xi_1/R \gtrsim 1$  and  $R/\delta \lesssim 1$ . Then no boundary layer will exist and vorticity would extend over distances beyond particle size. Only for particles of size  $d_p \lesssim 400 \mu\text{m}$  the flow would be approximately of Stokes type ( $Re_1 \lesssim 1$ ). For larger particles and low frequencies ( $\xi_1/R \gtrsim 1$  and  $Re_1 \gtrsim 1$ ) non-linear acoustic streaming effects would be relevant. As seen in the numerical study reported in [33], intense non-linear effects yield an increase of the pressure drop across the bed and would expectedly decrease the minimum fluidization velocity. A careful study of this situation requires a numerical analysis in which the interaction between boundary layers within the granular bed is also considered. Interestingly, fig. 6a shows that, at high frequencies, fluidization can be achieved for  $\xi_1/R \lesssim 1$  (or, equivalently  $u_s \lesssim u_1$ ). Thus, if  $u_s/u_1 \sim 1$  is assumed as the criterion for the onset of convection, this result sug-

gests that above a certain frequency the bed will transit directly from the solid-plastic to the liquid-like fluidization regime. Alternatively, if  $\Gamma = \Gamma_c = 1$  is taken as the threshold non-dimensional acceleration for the onset of convection, a direct transition to fluidization might be expected for  $\Gamma_{mf} < 1$ , *i.e.* vibration frequencies larger than  $f_c = 2\sqrt{2}\pi\Lambda\Upsilon/\tau$ . For a fixed vibration frequency, this criterion would yield a critical particle size below which surface waves would be directly observed at  $\Gamma \sim 1$ .

Obviously, the effect of interstitial gas would be most important for fine particles as seen experimentally [44] but the relative influence of acoustic streaming in promoting fluidization gains relevance as particle size is increased. For  $R/\delta > 1$ , it is  $\Upsilon > 2$  and the minimum fluidization velocity will be notably decreased by acoustic streaming. According to fig. 6b that will be the case of particles larger than about  $700 \mu\text{m}$  for  $f > 20 \text{ Hz}$ . In the limit  $R/\delta \gg 1$  it is  $\Upsilon \simeq (2/9)(R/\delta)^2 \gg 1$  and  $\omega\tau/\Upsilon \simeq \rho_p/\rho$ . Thus,  $\Gamma_{mf} \sim \rho_p/(\rho\Lambda) \sim 10$  and  $u'_{1mf} \sim \rho_p g/(\rho\Lambda\omega) \sim 100/\omega \text{ m/s}$  converge to values remarkably independent of particle size. Enhanced drag by acoustic streaming leads in this limit to a great reduction of the minimum fluidization velocity. For example, in the case of  $1 \text{ cm}$  sized particles subjected to a  $10 \text{ Hz}$  oscillatory flow ( $R/\delta \simeq 10$ ), it is  $u'_{1mf} \simeq 2.8 \text{ m/s}$ , which is rather small as compared to  $u_{mf} \simeq 100 \text{ m/s}$  if acoustic streaming were not considered. Note however that a more careful study requires a numerical approach since

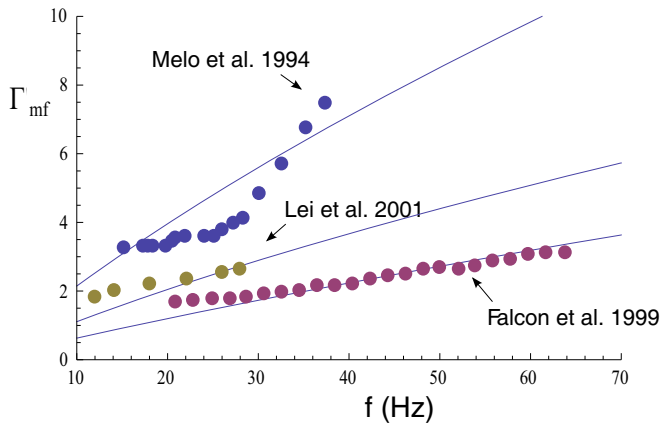


**Fig. 7.** Dimensionless acceleration at the onset of liquid-like surface waves in vibrated beds as a function of vibration frequency reported by Melo *et al.* [68] (200  $\mu\text{m}$  size spherical glass beads), Lei *et al.* [75] (200  $\mu\text{m}$  size quartz particles) and Falcon *et al.* [66] (120  $\mu\text{m}$  size irregularly shaped alumina grains). Solid lines represent the minimum fluidization dimensionless acceleration predicted by eq. (13) using  $\Psi = 1$ ,  $\phi = 0.35$ ,  $\rho_p = 3000 \text{ kg/m}^3$  [68];  $\Psi = 0.85$ ,  $\phi = 0.4$ ,  $\rho_p = 3000 \text{ kg/m}^3$  [75]; and  $\Psi = 0.8$ ,  $\phi = 0.4$ ,  $\rho_p = 4100 \text{ kg/m}^3$  [66].

non-linear effects would be relevant at these minimum fluidization conditions ( $\xi_{1mf}/R \sim 10$  and  $Re_{1mf} \sim 900$ ). The vibration amplitude needed to induce fluidization of deep beds of such large particles ( $\xi_{1mf} \simeq 5 \text{ cm}$ ) is not achievable in common lab scale experiments but intense oscillatory flows at large scales do exist in geological events involving either high energy shaking or sound waves that would yield acoustic streaming. Dynamical weakening in faults and landslides [93–95], triggering and fluidization of avalanches or liquefaction of soils by seismic waves [96] are representative geologic processes in which solid granular materials exhibit convective and liquid-like flows under apparently low shear stresses. Even though the elastic energy released by high frequency vibrations generated during soil failure is considered in some studies as responsible of dynamical weakening (acoustic fluidization [93]) the fundamental mechanisms governing the behavior of these oscillatory granular flows are still a subject of debate. The role of acoustic streaming remains yet to be explored. Our analysis suggests that acoustic streaming would help fluidization of relatively large particles at not excessively large vibration velocities by notably enhancing the fluid-solid hydrodynamic interaction.

### 3.4 The role of cohesiveness

A further parameter that merits a brief discussion is the cohesiveness of the granular material, which will be important for particles of size smaller than about 50  $\mu\text{m}$  [58]. The minimum fluidization velocity for beds of fine particles is very small (less than 1 cm/s) even though cohesiveness promotes the formation of strong aggregates and enduring gas channels that prevent uniform fluidization. On the other hand, it must be taken into account that

the particle relaxation time  $\tau$  is typically smaller than the oscillation period for these fine particles, which are therefore easily entrained in the gas flow oscillations. Thus, although not acting as obstacles to oscillations for acoustic streaming to be developed on their surface, the application of sound waves or vibration help the fluidization of fine particles by strongly agitating them, which destabilizes gas channels and breaks aggregates [97–101]. Some coarse granular materials may still acquire a cohesive nature if high levels of humidity are present, which gives rise to attractive capillary forces between the particles [102]. This is the case of unsaturated soils where the minimum fluidization velocity would be increased depending on the level of cohesion. A familiar example of cohesion induced by humidity is wet sand where typical values of the inter-particle capillary force can exceed particle weight in two or three orders of magnitude [103]. If however the level of water is increased, cohesion drops abruptly as the point of saturation is approached and water fills the pores of the material.

## 4 Conclusions

The fundamental physics that drives convection and fluidization of vibrated beds of large inertia particles remains elusive. Experience shows that the interaction of the interstitial gas with the solid particles is essential in many situations for the onset of convection and the transition to a liquid-like behavior. Moreover, the inertial convective regime is characterized by the formation of surface heaps sustaining an angle with the horizontal significantly smaller than the dynamic friction angle of the material (in the presence of interstitial gas), which is indicative of frictional weakening induced by hydrodynamic interactions. However, it is usually presumed that the critical oscillation velocities are very small as for the drag force exerted by the interstitial gas on the particles to have any significant influence. The present work is a first attempt to assess whether acoustic streaming arising from oscillatory viscous flows through granular beds might play a role on the onset of convection and fluidization in vertically vibrated granular beds.

Acoustic streaming appears whenever a viscous fluid oscillates in the presence of a solid boundary. The dissipation of energy by viscous friction leads to a secondary steady circulation of fluid in a boundary layer nearby the surface of the solid. For oscillation displacement amplitudes of the order of particle size (or, equivalently, dimensionless vibration energy comparable to dimensionless acceleration) the characteristic streaming velocity becomes comparable to the oscillation velocity. As seen from numerical simulations reported elsewhere, the streaming flow developed between oscillating spheres causes a tangential force on the particles aligned at an angle with the direction of oscillation. When the amplitude of the oscillations is similar to the radius of the spheres, this hydrodynamic shear force drives the formation of patterns in a horizontally vibrated layer of particles. In a vertically vibrated granular bed, it may be expected that the hydrodynamic

shear force would weaken the frictional resistance of the bed, thus triggering convection and the development of surface heaps with slope angles smaller than the characteristic dynamic friction angle in the absence of vibration. Furthermore, acoustic streaming may promote significantly the transfer of momentum from the fluid to the solids, which leads to a notable increase of the fluid rms pressure drop and therefore a decrease of the minimum fluidization velocity. The estimations carried out in this work show that fluidization of beds of relatively large particles could be enhanced by oscillatory flows at not too large Reynolds numbers giving rise to the observed liquid-like behavior.

The study of non-linear hydrodynamics when the amplitude of oscillations is much larger than particle size and the Reynolds number is large requires certainly a numerical study. Since it is generally impossible to solve the exact conservation equations for real situations, numerical codes commonly used to simulate granular flows are built up on two-phase models based on averaging the microscopic exact equations over a finite size volume that contains both phases. The averaging volume is much smaller than the system size yet large as compared to the typical size of the interfacial micro-structures. Gas-solid transfer terms such as the drag and heat/mass transfer coefficients and effective properties of the granular material are incorporated into the models from constitutive relationships empirically inferred. However, volume averaging precludes the analysis of microscopic phenomena occurring at the pore scale such as acoustic streaming. A preferable approach to get a grip on the fundamental physics that drives the non-linear streaming behavior of vibrated granular beds would be to solve the microscopic momentum and mass conservation equations (exact equations without phenomenological parameters) for simplified systems. Hopefully, this work will serve to encourage future experimental and numerical studies aimed at analyzing the effect of acoustic streaming on promoting frictional weakening and fluidization in vibrated granular beds.

Financial support by the Andalusian Regional Government (Junta de Andalucía, contract FQM-5735) and Spanish Government Agency Ministerio de Economía y Competitividad (contract CTQ2014-52763-C2-2-R) are acknowledged.

## References

1. M. Faraday, Philos. Trans. R. Soc. London **52**, 299 (1831).
2. Sedley Taylor, Proc. R. Soc. London **27**, 71 (1878).
3. V. Dvorak, Ann. Phys. **227**, 634 (1874).
4. E.N. da C. Andrade, Proc. R. Soc. London, Ser A **134**, 445 (1931).
5. B.A. Al-Zaitone, C. Tropea, Chem. Engin. Sci. **66**, 3914 (2011).
6. Lord Rayleigh, Philos. Trans. R. Soc. London **175**, 1 (1884).
7. Henk Jan van Gerner, Ko van der Weele, Martin A. van der Hoef, Devaraj van der Meer, J. Fluid Mech. **689**, 203 (2011).
8. H. Schlichting, Phys. Z. **33**, 327 (1932).
9. Peter J. Westervelt, J. Acous. Soc. Am. **25**, 60 (1953).
10. J. Holtmark, I. Johnsen, T. Sikkeland, S. Skavlem, J. Acous. Soc. Am. **26**, 26 (1954).
11. N. Riley, Q. J. Mech. Appl. Math. **19**, 461 (1966).
12. B.J. Davidson, N. Riley, J. Fluid Mech. **53**, 287 (1972).
13. A. Gopinath, A.F. Mills, ASME: J. Heat Transf. **115**, 332 (1993).
14. Chun P. Lee, Taylor G. Wang, J. Acoust. Soc. Am. **88**, 2367 (1990).
15. E.H. Trinh, J.L. Robey, Phys. Fluids **6**, 3567 (1994).
16. S.V. Komarov, *Advanced Topics in Mass Transfer, chapter Application of Airborne Sound Waves for Mass Transfer Enhancement* (InTech, 2011) pp. 61–86.
17. J.M. Valverde, J.M.P. Ebri, M.A.S. Quintanilla, Environ. Sci. Technol. **47**, 9538 (2013).
18. Steven L. Garrett, Am. J. Phys. **72**, 11 (2004).
19. F.H. Reynst, *Pulsating combustion: the collected works of F.H. Reynst* (Pergamom Press, 1961).
20. J.O. Gagnon, M.P. Paidoussis, J. Fluids Struct. **8**, 293 (1994).
21. A.L. Yarin, G. Brenn, O. Kastner, D. Rensink, C. Tropea, J. Fluid Mech. **399**, 151 (1999).
22. Frieder Mugele, Adrian Staicu, Rina Bakker, Dirk van den Ende, Lab Chip **11**, 2011 (2011).
23. Martin Wiklund, Roy Green, Mathias Ohlin, Lab Chip **12**, 2438 (2012).
24. Po-Chuan Huang, Chih-Cheng Chen, Hsiu-Ying Hwang, Int. J. Heat Mass Transfer **61**, 696 (2013).
25. N. Riley, Annu. Rev. Fluid Mech. **33**, 43 (2001).
26. Greg W. Swift, *Thermoacoustics: A Unifying Perspective for Some Engines and Refrigerators* (Acoustical Society of America through the American Institute of Physics, 2002).
27. S. Yavuzkurt, M.Y. Ha, G. Reethof, G. Koopmann, A.W. Scaroni, J. Energy Res. Technol. **113**, 286 (1991).
28. A. Gopinath, H.R. Harder, Int. J. Heat Mass Transt. **43**, 505 (2000).
29. Yonglin Ju, Yan Jiang, Yuan Zhou, Cryogenics **38**, 649 (1998).
30. B.P.M. Helvensteijn, A. Kashani, A.L. Spivak, P.R. Roach, J.M. Lee, and P. Kittel, in *Advances in Cryogenic Engineering*, Vol. **43** edited by P. Kittel (Springer US, 1998) pp. 1619–1626.
31. Melda Ödinc Çarpınlioglu, Mehmet Yasar Gündogdu, Flow Meas. Instrum. **12**, 163 (2001).
32. Li wen Jin, KaiChoong Leong, Transport Porous Media **72**, 37 (2008).
33. J.M. Valverde, F.J. Duran-Olivencia, Riv. Nuovo Cimento **37**, 591 (2014).
34. L.D. Landau, E.M. Lifshitz, *Course of Theoretical Physics*, chapter *Fluid Mechanics* (Pergamon Press, New York, 1995).
35. Jose Manuel Valverde, Contemp. Phys. doi:10.1080/00107514.2015.1008742(0):1–21, 0.
36. Sungryel Choi, Kwanwoo Nam, Sangkwon Jeong, Cryogenics **44**, 203 (2004).
37. D. Klotsa, Michael R. Swift, R.M. Bowley, P.J. King, Phys. Rev. E **79**, 021302 (2009).
38. R. Wunenburger, V. Carrier, Y. Garrabos, Phys. Fluids **14**, 2350 (2002).
39. C. Laroche, S. Douady, S. Fauve, J. Phys. (Paris) **50**, 699 (1989).

40. R. Evesque, J. Phys. (Paris) **51**, 697 (1990).
41. P. Evesque, Contemp. Phys. **33**, 245 (1992).
42. D.-W. Wang, Y.-C. Chou, T.-M. Hong, Europhys. Lett. **35**, 333 (1996).
43. Igor S. Aranson, Lev S. Tsimring, Rev. Mod. Phys. **78**, 641 (2006).
44. H. Pak, E. Van Doorn, R.P. Behringer, Phys. Rev. Lett. **74**, 4643 (1995).
45. M.H.I. Baird, M.G. Senior, R.J. Thompson, Chem. Engin. Sci. **22**, 551 (1967).
46. E.B. Tunstall, G. Houghton, Chem. Engin. Sci. **23**, 1067 (1968).
47. Yong Deng, Mooson Kwauk, Chem. Engin. Sci. **45**, 483 (1990).
48. T.S. Zhao, P. Cheng, Cryogenics **36**, 333 (1996).
49. J.A.C. Gallas, H.J. Herrmann, S. Sokolowski, Phys. Rev. Lett. **69**, 1371 (1992).
50. Y.-h. Taguchi, Phys. Rev. Lett. **69**, 1367 (1992).
51. J.J. Moreau, in *Powders Grains 93*, edited by C. Thornton (Balkema, Rotterdam, 1993) p. 227.
52. S. Luding, E. Clément, A. Blumen, J. Rajchenbach, J. Duran, Phys. Rev. E **50**, R1762 (1994).
53. Henk Jan van Gerner, Martin A. van der Hoef, Devaraj van der Meer, Ko van der Weele, Phys. Rev. E **76**, 051305 (2007).
54. Henk Jan van Gerner, Gabriel A. Caballero-Robledo, Devaraj van der Meer, Ko van der Weele, Martin A. van der Hoef, Phys. Rev. Lett. **103**, 028001 (2009).
55. J. Li, I.S. Aranson, W.-K. Kwok, L.S. Tsimring, Phys. Rev. Lett. **90**, 134301 (2003).
56. Stuart B. Savage, J. Fluid Mech. **194**, 457 (1988).
57. P. Evesque, E. Szmatala, J.-P. Denis, Europhys. Lett. **12**, 623 (1990).
58. Jose Manuel Valverde, *Fluidization of Fine Powders: Cohesive versus Dynamical Aggregation*, Vol. **18 Particle Technology Series** (Springer, 2013).
59. R.D. Wildman, J.M. Huntley, D.J. Parker, Phys. Rev. E **63**, 061311 (2001).
60. G. D'Anna, P. Mayor, A. Barrat, V. Loreto, Franco Nori, Nature **424**, 909 (2003).
61. Heinrich M. Jaeger, Sidney R. Nagel, Robert P. Behringer, Rev. Mod. Phys. **68**, 1259 (1996).
62. M. Nakagawa, S.A. Altobelli, A. Caprihan, E. Fukushima, E.K. Jeong, Exp. Fluids **16**, 54 (1993).
63. A. Castellanos, J.M. Valverde, A.T. Perez, A. Ramos, P.K. Watson, Phys. Rev. Lett. **82**, 1156 (1999).
64. J.M. Valverde, A. Castellanos, M.A.S. Quintanilla, Contemp. Phys. **44**, 389 (2003).
65. R.P. Behringer, E. van Doorn, R.R. Hartley, H.K. Pak, Granular Matter **4**, 9 (2002).
66. E. Falcon, K. Kumar, K. Bajaj, J.K. Bhattacharjee, Phys. Rev. E **59**, 5716 (1999).
67. H. Pak, R.P. Behringer, Phys. Rev. Lett. **71**, 1832 (1993).
68. F. Melo, P. Umbanhowar, H.L. Swinney, Phys. Rev. Lett. **72**, 172 (1994).
69. Benku Thomas, Arthur M. Squires, Phys. Rev. Lett. **81**, 574 (1998).
70. J. Duran, Phys. Rev. Lett. **84**, 5126 (2000).
71. R.J. Milburn, M.A. Naylor, A.J. Smith, M.C. Leaper, K. Good, Michael R. Swift, P.J. King, Phys. Rev. E **71**, 011308 (2005).
72. P. Evesque, J. Rajchenbach, Phys. Rev. Lett. **62**, 44 (1989).
73. Eric van Doorn, R.P. Behringer, Phys. Lett. A **235**, 469 (1997).
74. Francisco Melo, Paul B. Umbanhowar, Harry L. Swinney, Phys. Rev. Lett. **75**, 3838 (1995).
75. Sui Lei, Miao Guo-Qing, Wei Rong-Jue, Chin. Phys. Lett. **18**, 614 (2001).
76. P.C. Carman, Chem. Engin. Res. Design **75**, S32 (1997).
77. K. Rietema, *The Dynamics of Fine Powders* (Elsevier, London, 1991).
78. M.L. Hunt, C.R. Wassgren, C.E. Brennen, J. Appl. Mech. **63**, 712 (1996).
79. J.M. Valverde, A. Castellanos, Europhys. Lett. **75**, 985 (2006).
80. R.L. Brown, J.C. Richards, P.V. Danckwerts, *Principles of Powder Mechanics: Essays on the Packing and Flow of Powders and Bulk Solids* (Elsevier Science, 2013).
81. W.C. Yang, *Handbook of Fluidization and Fluid-Particle Systems* (Taylor & Francis, 2003).
82. A.C. Hoffmann, H.J. Finkers, Powder Technol. **82**, 197 (1995).
83. E.R. Nowak, J.B. Knight, E. Ben-Naim, H.M. Jaeger, S.R. Nagel, Phys. Rev. E **57**, 1971 (1998).
84. Osborne Reynolds, Philos. Mag. Ser. 5 **20**, 469 (1885).
85. Sandra Wegner, Ralf Stannarius, Axel Boese, Georg Rose, Balazs Szabo, Ellak Somfai, Tamas Borzsonyi, Soft Matter **10**, 5157 (2014).
86. E. van Doorn, R.P. Behringer, Europhys. Lett. **40**, 387 (1997).
87. Jose Manuel Valverde, Soft Matter **9**, 8792 (2013).
88. P.B. Umbanhowar, F. Melo, H.L. Swinney, Nature **382**, 793 (1996).
89. P.B. Umbanhowar, F. Melo, H.L. Swinney, Physica A **249**, 1 (1998).
90. S. Douady, S. Fauve, C. Laroche, Europhys. Lett. **8**, 621 (1989).
91. John R. de Bruyn, B.C. Lewis, M.D. Shattuck, Harry L. Swinney, Phys. Rev. E **63**, 041305 (2001).
92. Osamu Sano, Ataka Takei, AIP Conf. Proc. **1145**, 729 (2009).
93. H.J. Melosh, Nature **379**, 601 (1996).
94. Kaiwen Xia, Sheng Huang, Chris Marone, Geochem. Geophys. Geosyst. **14**, 1012 (2013).
95. Antoine Lucas, Anne Mangeney, Jean Paul Ampuero, Nat. Commun. **5**, 3417 (2014).
96. Alexander Wong, Chi-Yuen Wang, J. Geophys. Res. B: Solid Earth **112**, B10305 (2007).
97. R. Chirone, L. Massimilla, S. Russo, Chem. Engin. Sci. **48**, 41 (1993).
98. A. Ajbar, Y. Bakhbakhi, S. Ali, M. Asif, Powder Technol. **206**, 327 (2011).
99. P. Ammendola, R. Chirone, F. Raganati, Chem. Engin. Proc.: Proc. Intensif. **50**, 885 (2011).
100. J.M. Valverde, F. Raganati, M.A.S. Quintanilla, J.M.P. Ebri, P. Ammendola, R. Chirone, Appl. Energy **111**, 538 (2013).
101. F. Raganati, P. Ammendola, R. Chirone, Appl. Energy **113**, 1269 (2014).
102. C. Soria-Hoyo, J.M. Valverde, A. Castellanos, Powder Technol. **196**, 257 (2009).
103. H. Schubert, Powder Technol. **37**, 105 (1984).
104. M. Campbell, J.A. Cosgrove, C.A. Greated, S. Jack, D. Rockliff, Optics Laser Technol. **32**, 629 (2000).



Prof. José Manuel Valverde Millán obtained a Bachelor Science degree in Physics at the University of Seville in Spain in 1993, and a Ph.D. in Physics from the same University in 1997. He is currently Professor and Researcher at the University of Seville. His research activity has been focused on the study of fluidization and mechanical properties of granular materials and can be considered as highly inter- or multi-disciplinary, lying between the areas of engineering and fundamental physics. A main subject of current interest is the development of novel techniques to enhance the CO<sub>2</sub> capture and thermochemical energy storage efficiencies of CaO-based materials by means of the Ca-looping technology based on carbonation/calcination of natural limestone and dolomite in fluidized beds.